arXiv:cond-mat/0507729v1 [cond-mat.other] 29 Jul 2005

Threshold behavior of bosonic two-dimensional few-body systems

D. Blume[1]

[1]*Department of Physics and Astronomy, Washington State University, Pullman, Washington 99164-2814*

(Dated: March 23, 2022)

Bosonic two-dimensional self-bound clusters consisting of N atoms interacting through additive van der Waals potentials become unbound at a critical mass $m_*^{(N)}$; $m_*^{(N)}$ has been predicted to be independent of the size of the system. Furthermore, it has been predicted that the ground state energy E_N of the N-atom system varies exponentially as the atomic mass approaches m_*. This paper reports accurate numerical many-body calculations that allow these predictions to be tested. We confirm the existence of a universal critical mass m_*, and show that the near-threshold behavior can only be described properly if a previously neglected term is included. We comment on the universality of the energy ratio E_{N+1}/E_N near threshold.

PACS numbers:

Restricting the motion of particles to one or two dimensions can lead to properties that differ dramatically from those in three dimensions. The most prominent two-dimensional (2D) system is the surface of bulk matter. Another example are one- or two-atom layer thin films, e.g., atomic or molecular hydrogen films [1, 2], grown on substrates. Neglecting the adatom-substrate interaction, many properties of such systems can be understood within a truly 2D framework. In addition to homogeneous 2D systems, it is interesting to consider 2D clusters (see, e.g., Refs. [3, 4]). What happens when a finite number of atoms is restricted to 2D space? Inhomogeneous 2D systems can potentially be studied by placing a few atoms on the surface of a substrate or by confining atoms by external potentials. Effectively 2D atom traps have been realized recently [5, 6]; extension to optical lattices with only a few atoms per lattice site is possible with today's technology. These systems are particularly interesting since Feshbach resonances allow the interaction strengths to be tuned through application of magnetic fields.

Bosonic 2D systems interacting through short-range two-body potentials that support one zero angular momentum bound state are predicted to exhibit intriguing universal, that is, model-independent, behaviors [7, 8, 9, 10, 11, 12, 13, 14, 15, 16, 17, 18]. i) 2D clusters with N particles [9, 10, 12] are predicted to become unbound when the mass m reaches a critical value $m_*^{(N)}$ [7]. This critical mass is predicted to be universal, i.e., $m_*^{(N)} = m_*$ [10], and to be the same for the corresponding homogeneous system [8, 19]. ii) For a given system size, the ground state energies E_N near threshold are predicted to change exponentially as the atomic mass m decreases [7, 11]. Similarly, for a given atomic mass, the ground state energies near threshold are predicted to change exponentially with varying system size [17]. iii) The ratio between the ground state energies of a 2D system with $N+1$ atoms and those of a system with N atoms reaches, in the limit of zero-range interactions, a constant. This constant has been determined analytically for small 2D systems: $E_3^\delta/E_2^\delta = 16.52$ [9, 16] and $E_4^\delta/E_3^\delta = 11.94$ [18]. For large systems, the ratio $E_{N+1}^\delta/E_N^\delta$ has been predicted to approach 8.57 [17]. These predictions should apply to systems interacting through short-range potentials if $|E_N| \ll \hbar^2/(mr_e^2)$, where r_e denotes the maximum of the characteristic length of the two-body potential [in our case, the van der Waals length $r_{\rm vdW}$, $r_{\rm vdW} = (mC_6/\hbar^2)^{1/4}$, where C_6 denotes the leading van der Waals coefficient] and the absolute value of the effective range $r_{\rm eff}$.

This paper reports the energetics of self-bound inhomogeneous 2D systems near threshold, and tests under which conditions predictions i) to iii) apply. To this end we perform numerical many-body calculations, which supersede earlier variational calculations [10, 11] and cover a wider parameter range. For $N = 2$ and 3 we determine the ground state energy using basis set expansion-type calculations. Since these techniques become untractable for larger systems, we resort to Monte Carlo techniques for $N > 3$. We show that a proper description of the ground state energies for small clusters with $N = 2 - 5$ atoms near threshold requires, in addition to a term proportional to $(m - m_*^{(N)})$, a term proportional to $(m - m_*^{(N)})^2$. For larger droplets with $N = 6$ and 7 atoms we only include the linear term; our diffusion Monte Carlo (DMC) energies do not allow the term proportional to $(m-m_*^{(N)})^2$ to be determined. We speculate that DMC energies covering a larger mass range (see below) would show that near threshold the quadratic term is non-negligible for systems with $N \geq 6$. Our study confirms the existence of a universal critical mass m_* [10]. This critical mass depends on the two-body potential but appears to be universal for bosonic N-particle systems interacting additively through a given two-body potential. Finally, we investigate the ratio between the total ground state energy of 2D systems with $N + 1$ and N particles. Our results are consistent with predictions based on zero-range treatments [9, 16, 17, 18] but do not conclusively confirm them for $N > 3$. We comment on the relevance

of the energy scale associated with the effective range.

Consider the Hamiltonian H for N particles with mass m,

$$H = -\frac{\hbar^2}{2m}\sum_{i=1}^{N}\nabla_i^2 + \sum_{i<j}^{N} V(r_{ij}), \qquad (1)$$

where ∇_i^2 denotes the 2D Laplace operator of the ith particle, r_{ij} the distance between atom i and j, and V the atom-atom potential. We use the realistic helium-helium potential without retardation developed by Korona *et al.* [20] (in the following referred to as KORONA potential) as well as a Lenard-Jones (LJ) potential with parameters ϵ and σ chosen to approximate the helium dimer interaction, i.e., $\epsilon = 10.22$ K and $\sigma = 2.56$ Å [21]. Both these two-body potentials support a single two-body bound state with vanishing angular momentum. In the following, we calculate the lowest energy with vanishing angular momentum of the many-body system. We first treat "true" bosonic helium systems in 2D, i.e., we choose $m = m_{\rm He}$ (here and in the following, He denotes the isotope ^{4}He). To explore the threshold regime, we then successively reduce the atomic mass while leaving the interaction potential unchanged.

To start with, we solve the scaled radial Schrödinger equation for two atoms by diagonalizing the Hamiltonian using B-splines. For each mass, the adaptive grid and box-size are optimized [22]. When we vary the atomic mass from $m/m_{\rm He} = 1$ to 0.692, the two-body binding energy E_2 for the KORONA potential changes by nearly ten orders of magnitude from $E_2 = -0.041$ K to $E_2 = -8.6\times10^{-12}$ K. The total ground state energies E_N for a given N near threshold, scaled by the atom mass m, are predicted to vary exponentially as a function of m [7],

$$mE_N \propto \exp\left\{-\left[\sum_{i=1}^{\infty} a_i^{(N)}\left(\frac{m}{m_{\rm He}} - \frac{m_*^{(N)}}{m_{\rm He}}\right)^i\right]^{-1}\right\}. \qquad (2)$$

Here, $m_*^{(N)}$ denotes the critical mass at which the N-body system becomes unbound, and $a_i^{(N)}$ parameters specific to the N particle system. The mass m is directly proportional to the coupling strength K and inversely proportional to the quantum parameter η, which have been used previously to characterize LJ systems (see [21]). The functional form in Eq. (2) has been derived by Taylor-expanding the logarithmic derivative of the bound state wave function for small total ground state energies about $(m_*^{(N)} - m)$ [7]. Previous treatments neglected terms proportional to $(m_*^{(N)} - m)^i$ with $i > 1$. To test whether this is justified, symbols in Fig. 1 show the quantity $-1/\ln(m|E_2|/m_{\rm He}\epsilon)$, where ϵ denotes the well depth of the KORONA and LJ potential, respectively, as a function of $m/m_{\rm He}$ ($\epsilon = 11.06$ K for the KORONA potential and 10.22 K for the LJ potential). Diamonds show the ground state energies for the dimer interacting through the KORONA potential, and asterisks those for the dimer interacting through the LJ potential. Figure 1 shows clear deviations from a linear behavior, indicating that the term proportional to $(m - m_*^{(2)})^2$ cannot be neglected for $N = 2$. Earlier studies [10, 11, 12] did not see deviations from the linear behavior possibly because the total ground state energies were i) varied over a smaller range, and ii) determined variationally. The qualitative behavior of the energies calculated using the KORONA and the LJ potential is similar, which implies that the non-linear behavior cannot be attributed to the difference in the long-range parametrization of the two two-body potentials [the LJ potential is for large r proportional to r^{-6}, while the KORONA potential contains additional terms proportional to r^{-j}, where $j = 8 - 16$ (j even)].

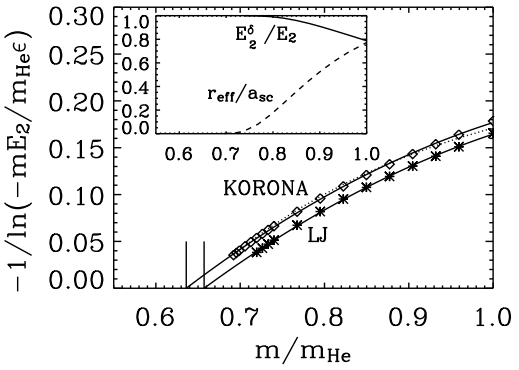


FIG. 1: Scaled ground state energies $-1/\ln(m|E_2|/m_{\rm He}\epsilon)$ for two 2D particles interacting through the KORONA potential (diamonds) and through a simple LJ potential (asterisks) as a function of $m/m_{\rm He}$. Solid lines show fits, which treat $m_*^{(2)}$, $a_1^{(2)}$ and $a_2^{(2)}$ as parameters. Vertical solid lines indicate the mass ratio $m_*^{(2)}/m_{\rm He}$ at which the fit predicts the dimer to become unbound. The dotted line shows E_2^δ, Eq. (3), for the dimer interacting through the KORONA potential. The inset shows the ratios between the energies E_2^δ and E_2 (solid line), and between $r_{\rm eff}$ and a_{sc} (dashed line) for two particles interacting through the KORONA potential as a function of $m/m_{\rm He}$.

Solid lines in Fig. 1 show fits of our scaled numerical two-body ground state energies to Eq. (2), treating $m_*^{(2)}$, $a_1^{(2)}$ and $a_2^{(2)}$ as fitting parameters and setting $a_i^{(2)}$ with $i > 2$ to zero. The fits predict that the two-body system interacting through the KORONA potential becomes unbound at $m_*^{(2)} = 0.636(3)m_{\rm He}$ and that interacting through the LJ potential at $m_*^{(2)} = 0.657(3)m_{\rm He}$. The numbers in brackets denote the uncertainties of the fit, which are obtained by including a varying number of data points in the fit. Table I lists the fitting parameters

$m_*^{(2)}$, $a_1^{(2)}$ and $a_2^{(2)}$ and their uncertainties. The critical masses $m_*^{(2)}$ for both interaction potentials are indicated in Fig. 1 by vertical solid lines.

It is interesting to ask how well effective range theory describes the near-threshold behavior of the 2D dimer. For a zero-range potential, the ground state energy E_2^δ is determined by the 2D scattering length a_{sc} (see, e.g., Ref. [16]),

$$E_2^\delta = -\frac{\hbar^2}{m a_{sc}^2}\, 4\exp(-2C), \tag{3}$$

where C denotes Euler's constant, $C = 0.5772$. Our definition of the scattering length a_{sc} follows that adopted by Verhaar *et al.* [23], that is, the scattering wave function goes through zero at $r = a_{sc}$. In the following we restrict ourselves to dimers interacting through the KORONA potential. The scattering length a_{sc}, which we determine numerically, varies from 77.8 Å for the 2D helium dimer to about 5.7×10^6 Å for the most weakly-bound dimer considered with $m = 0.692 m_{\rm He}$. A dotted line in Fig. 1 shows E_2^δ, Eq. (3), using scaled dimensionless units. Near threshold, E_2^δ nearly coincides with the numerically determined energy E_2 (diamonds). At larger m, however, discrepancies are visible. To quantify these discrepancies, a solid line in the inset of Fig. 1 shows the energy ratio E_2^δ/E_2, which varies from essentially 1 to 0.8 for the atomic masses considered. Near threshold, the ground state energy E_2 can be described to a very good approximation through a single atomic physics parameter, i.e., the two-body scattering length a_{sc}; the importance of effective range corrections, however, increases with increasing mass.

To account for a non-vanishing effective range, the right hand side of Eq. (3) has to be multiplied by $\exp(|E_2|\, m r_{\rm eff}^2/(4\hbar^2))$ [23, 24]. The effective range $r_{\rm eff}$,

$$r_{\rm eff} = 2\sqrt{\frac{\hbar^2}{|E_2| m} \ln\left(|E_2| \frac{m a_{sc}^2}{\hbar^2} \frac{\exp(2C)}{4}\right)}, \tag{4}$$

can hence be evaluated if the scattering length a_{sc} and the binding energy E_2 are known. For the dimers under study, $r_{\rm eff}$ changes from 60 Å for $m/m_{\rm He} = 1$ to 4900 Å for $m = 0.696 m_{\rm He}$. For smaller masses the numerical accuracy of E_2 and a_{sc} is not sufficient to reliably determine $r_{\rm eff}$ from Eq. (4). A dashed line in the inset of Fig. 1 shows the ratio between $r_{\rm eff}$ and a_{sc}. Since the effective range $r_{\rm eff}$ increases with decreasing atomic mass, the energy scale associated with the effective range $r_{\rm eff}$, $\hbar^2/(m r_{\rm eff}^2)$ [25], decreases with decreasing m (see below).

We now turn to the study of 2D trimers interacting additively through the KORONA potential. Since the potential energy depends on relative coordinates only, we can separate off the center of mass motion. Restricting ourselves to states with vanishing total angular momentum reduces the number of degrees of freedom to three. The 2D Schrödinger equation can then be rewritten in terms of three hyperspherical coordinates. Here, we employ Whitten-Smith's democratic coordinates R, ϑ and φ [26]. We determine the solution to the Schrödinger equation by first calculating a set of angular-dependent channel functions and then solving a set of coupled hyperradial equations. Since our B-spline implementation closely follows that used in Ref. [27] for 3D trimers, we do not discuss it in detail here. We note, however, that the grandangular momentum operator in 2D differs from that in 3D (see, e.g., Ref. [28]) and that the range of the angular coordinate ϑ changes from $[0, \pi/4]$ in 3D to $[-\pi/4, \pi/4]$ in 2D [28, 29]. We include up to twelve channels in our calculations and estimate the uncertainty of the ground state energy E_3, which, in addition to the number of channels included in the expansion, depends on the angular and radial grids employed and on the step size ΔR used to calculate the coupling matrix elements [27], to be at the few percent level.

Asterisks in Fig. 2(a) show the ground state energies $|E_3|$ on a log-scale as a function of the scaled mass $m/m_{\rm He}$. Since the system size increases with decreasing mass, the calculations become more involved as the mass decreases. For the masses considered, the total ground state energy varies over nearly four orders of magnitude from $E_3 = -0.180$ K for $m/m_{\rm He} = 1$ to $E_3 = -6.51 \times 10^{-5}$ K for $m/m_{\rm He} = 0.740$. To test the applicability of Eq. (2), asterisks in Fig. 2(b) show the scaled gound state energies $-\ln(m|E_3|/m_{\rm He}\epsilon)$ as a function of the scaled mass $m/m_{\rm He}$. As in the $N = 2$ case, the scaled energies for $N = 3$ clearly show deviations from linear behavior. To determine the critical mass for the trimer system, we fit our data to Eq. (2) treating $m_*^{(3)}$, $a_1^{(3)}$ and $a_2^{(3)}$ as fitting parameters. Table I summarizes the result of the fit, which is shown by a solid line in Fig. 2(b). The uncertainties of the fit are, as in the dimer case, determined by including a varying number of data points in the fit. Notably, the predicted critical mass $m_*^{(3)}$ for the trimer interacting additively through the KORONA potential nearly coincides with the critical mass $m_*^{(2)}$ for the dimer interacting through the KORONA potential.

We now consider 2D systems with up to $N = 7$ particles interacting additively through the KORONA potential. For these larger systems, basis set expansion-type techniques become computationally unfeasible. We thus solve the 2D many-body Schrödinger equation by alternative means using the essentially exact DMC technique with importance sampling [30]. The DMC technique allows ground state energies and structural properties to be determined. Since the numerical solution of the time-independent Schrödinger equation is based on a stochastic process, expectation values can only be determined within a statistical uncertainty. This statistical uncertainty can be reduced by increasing the computational

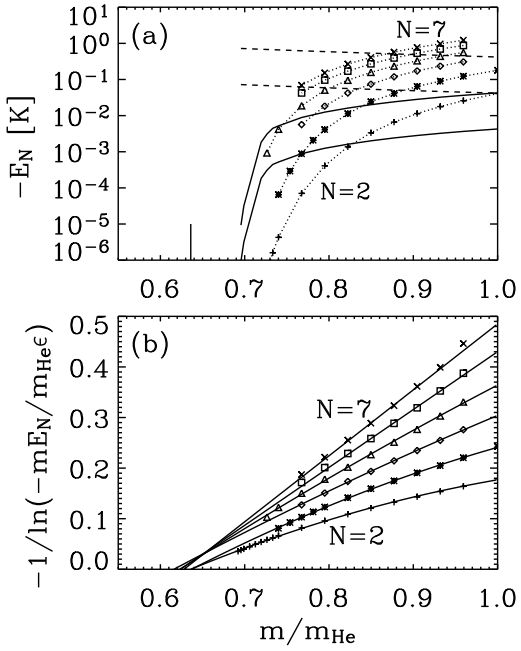


FIG. 2: (a) Symbols show the total ground state energies E_N for $N = 2$ (pluses), $N = 3$ (asterisks), $N = 4$ (diamonds), $N = 5$ (triangles), $N = 6$ (squares), and $N = 7$ (crosses) on a logarithmic scale as a function of $m/m_{\rm He}$ for the KORONA potential. Dotted lines connect data points for fixed N to guide the eye. The upper solid and dashed lines show $\hbar^2/(mr_e^2)$ for $r_e = r_{\rm eff}$ and $r_e = r_{\rm vdW}$, respectively. The lower solid and dashed lines show $0.1\hbar^2/(mr_e^2)$ for $r_e = r_{\rm eff}$ and $r_e = r_{\rm vdW}$, respectively. A vertical solid line indicates the mass ratio $m_*^{(2)}/m_{\rm He} = 0.636$, at which our fits predict the 2D dimer to become unbound; the critical masses for the larger systems nearly coincide with that for the dimer. (b) Scaled total ground state energies $-1/\ln(m|E_N|/m_{\rm He}\epsilon)$ as a function of $m/m_{\rm He}$ using the same symbols as in (a). Solid lines show fits (treating $m_*^{(N)}$, $a_1^{(N)}$ and $a_2^{(N)}$ as parameters for $N = 2-5$, and treating $m_*^{(N)}$ and $a_1^{(N)}$ as parameters for $N = 6-7$).

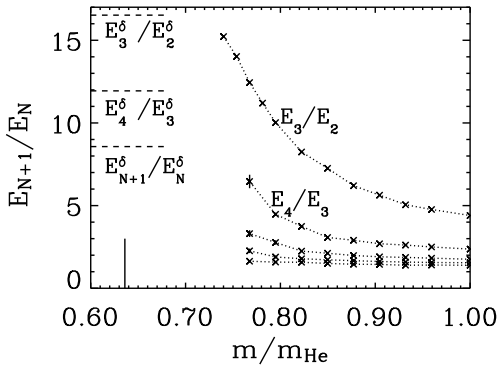


FIG. 3: Energy ratios E_{N+1}/E_N as a function of $m/m_{\rm He}$ for $N = 2$ (uppermost curve) through $N = 6$ (lowermost curve) calculated using the KORONA potential. Errorbars reflect the statistical uncertainties of our DMC energies E_N for $N \geq 4$. Dashed horizontal lines on the left hand side indicate the energy ratios for zero-range interactions: $E_3^\delta/E_2^\delta = 16.52$, $E_4^\delta/E_3^\delta = 11.94$ and $E_{N+1}^\delta/E_N^\delta = 8.57$. A vertical solid line indicates the mass ratio $m_*^{(2)}/m_{\rm He} = 0.636$, at which our fits predict the 2D dimer to become unbound. The critical masses for larger systems nearly coincide with that for the dimer.

efforts. Our DMC energies for the 2D helium trimer and tetramer agree with those calculated by Vranješ and Kilić [31]. Furthermore, our DMC energies for the trimer agree to within the statistical uncertainty with those calculated by the hyperspherical B-spline treatment (see above). In the following, we report the ground state energies E_N for $N > 3$ calculated by the DMC method as a function of the atomic mass. As we approach the threshold regime, the DMC calculations become more difficult since the kinetic and potential energy nearly cancel.

Symbols in Fig. 2 show the DMC ground state energies E_N as a function of the mass ratio $m/m_{\rm He}$ for $N = 4-7$. Panel (a) shows the energies on a logarithmic scale (to guide the eye dotted lines connect data points for the same N). To investigate how well the functional form given in Eq. (2) applies to systems with $N > 3$, panel (b) shows the scaled DMC ground state energies $-1/\ln(m|E_N|/m_{\rm He}\epsilon)$. Statistical uncertainties of the DMC energies (not shown) are smaller than the symbol size. Deviations from a linear behavior are, although less pronounced than for the dimer and trimer, visible for $N = 4$ and 5; consequently, we fit our DMC energies to Eq. (2), treating $m_*^{(N)}$, $a_1^{(N)}$ and $a_2^{(N)}$ as fitting parameters. For the clusters with $N = 6$ and 7, our scaled DMC energies depend to a good approximation linearly on the mass; hence we use only two fitting parameters, $m_*^{(N)}$ and $a_1^{(N)}$. The fitting parameters are summarized in Table I, and the fits are shown by solid lines in Fig. 2(b). The statistical uncertainty of the fits is, as in the dimer and trimer case, estimated by including a varying number of data points in the fit. We speculate that, if we were able to obtain accurate DMC energies closer to threshold, non-linear behavior of the scaled ground state energies for $N \geq 6$ would be, similarly as for the dimer and trimer, visible. The fits for $N = 4-7$ predict critical masses $m_*^{(N)}/m_{\rm He}$ between 0.62 and 0.63, which agree within their uncertainties with those predicted for $N = 2$ and 3. Our analysis thus confirms that the critical mass $m_*^{(N)}$ at which 2D systems, interacting additively through a given two-body potential, become unbound is the same for all system sizes [10, 11, 12].

To further investigate the near-threshold behavior for $N > 2$, symbols in Fig. 3 show the ratio between the ground state energies for systems with $N+1$ and N atoms

as a function of $m/m_{\rm He}$. To guide the eye, dotted lines connect data points for E_{N+1}/E_N with the same $N+1$ and N but different m. Errorbars, which increase with decreasing mass, reflect the statistical uncertainty of our DMC energies for $N \geq 4$. At large m, the energy ratios approach a constant, in agreement with earlier studies [12]. Since $|E_2|$ decreases with decreasing mass while the van der Waals length $r_{\rm vdW}$ changes only little [see dashed lines in Fig. 2(a)], dimers with small m effectively have a shorter range than those with large m. Accordingly, systems with small m should be better described by zero-range models than those with large m. Horizontal dashed lines on the left hand side of Fig. 3 indicate the energy ratios $E_3^\delta/E_2^\delta = 16.52$ [16], $E_4^\delta/E_3^\delta = 11.94$ [18] and $E_{N+1}^\delta/E_N^\delta = 8.57$ [17] for 2D systems interacting through additive zero-range potentials. While the energy ratio E_3/E_2 calculated for the helium-like few-body systems with small m is close to the value predicted by the zero-range treatment, none of the energy ratios E_{N+1}/E_N for $N \geq 3$ is. Although the energy ratios for $N \geq 3$ increase with decreasing mass, it is not clear whether they approach the values predicted for the zero-range model.

Recall that zero-range treatments should be applicable when the energy scale associated with r_e is much larger than $|E_N|$, where r_e is either given by the van der Waals length $r_{\rm vdW}$ or by the effective range $r_{\rm eff}$. Solid and dashed lines in panel (a) of Fig. 2 show the energy $\hbar^2/(mr_e^2)$ for $r_e = r_{\rm eff}$ (upper solid line) and for $r_e = r_{\rm vdW}$ (upper dashed line), respectively. Since $|E_N| \ll \hbar^2/(mr_e^2)$ for zero-range treatments to be valid, the lower solid and dashed lines show the quantity $0.1\,\hbar^2/(mr_e^2)$ for $r_e = r_{\rm eff}$ and $r_e = r_{\rm vdW}$, respectively. Figure 2(a) indicates that, of the systems considered, only those with $N = 2$ and 3 have total ground state energies $|E_N|$ that are smaller than the lower solid and dashed lines. Although the dimer near threshold is well described by a zero-range treatment (see Fig. 1), the corresponding systems with $N > 3$ cannot be properly described through simple contact interactions. This is due to the fact that the total ground state energies vary exponentially as a function of N and that the effective range $r_{\rm eff}$ increases with decreasing m. To check whether the latter is specific to the KORONA potential studied here, we also calculated the effective range $r_{\rm eff}$ for the LJ potential discussed above and for a realistic tritium-tritium $\mathrm{b}^3\Sigma_u^+$ potential. For the three potentials considered, the effective range behaves similarly as a function of the two-body binding energy. Our findings suggest that the regime where the N-body total ground state energies E_N, $N \gg 2$, can be properly described by zero-range models might, in general, be hard to reach for 2D van der Waals systems.

Finally we remark on an earlier variational study [3], which concluded that artificial "bosonic helium 3" clusters in 2D become bound for a minimum of about twelve atoms. Although the figures in this paper contain energies for $m \leq m(^3\mathrm{He})$ for only a few system sizes, our calculations show that bosonic ^{3}He clusters are self-bound for all N considered, in agreement with Ref. [31]. (We excluded some energies for small m from the figures and the fits since their statistical uncertainties are very large.) Furthermore, the existence of a universal critical mass m_* indicates that "bosonic helium 3" 2D clusters, which are often studied to complement the treatment of fermionic helium 3 systems, are bound for all N. Our calculations emphasize that great care has to be taken when variational calculations are used to investigate the near-threshold regime (see also Ref. [4]).

	N	$m_*^{(N)}$	$a_1^{(N)}$	$a_2^{(N)}$
LJ	2	0.657(3)	0.66(2)	-0.53(6)
KORONA	2	0.636(3)	0.68(2)	-0.55(6)
	3	0.637(8)	0.86(5)	-0.53(14)
	4	0.62(2)	0.89(8)	-0.25(12)
	5	0.62(2)	1.06(10)	-0.26(20)
	6	0.62(3)	1.14(10)	
	7	0.63(2)	1.30(7)	

TABLE I: Fitting parameters for 2D clusters interacting through the Lenard-Jones potential (for $N = 2$ only) and through the KORONA potential ($N = 2-7$), respectively. We treat three fitting parameters for $N = 2-5$, and two fitting parameters for $N = 6-7$. The numbers in brackets give the uncertainties of the fitting parameters, which are obtained by including a varying number of data points in the fit.

Fruitful discussions with H.-W. Hammer and D.T. Son, which motivated this work, and with C.H. Greene are gratefully acknowledged. Acknowledgement is made to the Donors of The Petroleum Research Fund, administered by the American Chemical Society, and the NSF (grant ITR-0218643) for support of this research.

[1] A. I. Safonov *et al.*, Phys. Rev. Lett. **81**, 4545 (1998).
[2] F.-C. Liu, Y.-M. Liu, and O. E. Vilches, Phys. Rev. B **51**, 2848 (1995).
[3] B. Krishnamachari and G. V. Chester, Phys. Rev. B **59**, 8852 (1999).
[4] A. Sarsa, J. Mur-Petit, A. Polls, and J. Navarro, Phys. Rev. B **68**, 224514 (2003).
[5] A. Görlitz *et al.*, Phys. Rev. Lett. **87**, 130402 (2001).
[6] D. Rychtarik *et al.*, Phys. Rev. Lett. **92**, 173003 (2004).
[7] A. Bagchi, Phys. Rev. A **3**, 1133 (1971).
[8] L. W. Bruch, Phys. Rev. B **13**, 2873 (1976).
[9] L. W. Bruch and J. A. Tjon, Phys. Rev. A **19**, 425 (1979).
[10] F. Cabral and L. W. Bruch, J. Chem. Phys. **70**, 4669 (1979).
[11] T. K. Lim, S. Nakaichi, Y. Akaishi, and H. Tanaka, Phys. Rev. A **22**, 28 (1980).
[12] J. A. Tjon, Phys. Rev. A **21**, 1334 (1980).
[13] S. K. Adhikari *et al.*, Phys. Rev. A **37**, 3666 (1988).

[14] S. K. Adhikari, A. Delfino, T. Frederico, and L. Tomio, Phys. Rev. A **47**, 1093 (1993).

[15] S. K. Adhikari, T. Frederico, and I. D. Goldman, Phys. Rev. Lett. **74**, 487 (1995).

[16] A. S. Jensen, K. Riisager, D. V. Fedorov, and E. Garrido, Rev. Mod. Phys. **76**, 215 (2004).

[17] H.-W. Hammer and D. T. Son, Phys. Rev. Lett. **93**, 250408 (2004).

[18] L. Platter, H.-W. Hammer, and U.-G. Meissner, Few-Body Systems **35**, 169 (2004).

[19] M. D. Miller and L. H. Nosanow, J. Low Temp. **32**, 145 (1978).

[20] T. Korona *et al.*, J. Chem. Phys. **106**, 5109 (1997).

[21] The calculations are performed using (all digits used in the calculation are reported) $m_{\rm He} = 7296.3$ m$_e$, $\epsilon = 10.22$ K, $\sigma = 2.56$ Å and $V_{LJ} = 4\epsilon[(r/\sigma)^{-12} - (r/\sigma)^{-6}]$. These parameters result in the dimensionless coupling constant $K = 22.11$ (rounded), where $K = 4m\epsilon\sigma^2/\hbar^2$, and the quantum constant $\eta = 0.1809$ (rounded), where $\eta = \hbar^2/(m\epsilon\sigma)$.

[22] The calculations require the maximum r value r_{max} to be chosen properly; to obtain full convergence r_{max} has to be roughly 100 times larger than the 2D two-body scattering length a_{sc} (see text). To converge our two-body energies, we space the grid points along the radial coordinate r using a $r^{1/n}$ grid, where n denotes an integer, $n = 1 - 8$ (the larger r_{max} the larger n). Convergence was tested by varying the number of grid points between 400 and 800.

[23] B. J. Verhaar, J. P. H. W. van den Eijnde, M. A. J. Voermans, and M. M. J. Schaffrath, J. Phys. A **17**, 595 (1984).

[24] H.-W. Hammer, private communication.

[25] In defining the energy scale associated with r_e we drop the factor $4\exp(-2C) = 1.2609$.

[26] R. C. Whitten and F. T. Smith, J. Math. Phys. **9**, 1103 (1968).

[27] D. Blume, C. H. Greene, and B. D. Esry, J. Chem. Phys. **113**, 2145 (2000).

[28] B. R. Johnson, J. Chem. Phys. **79**, 1916 (1983).

[29] B. R. Johnson, J. Chem. Phys. **73**, 5051 (1980).

[30] B. L. Hammond, W. A. Lester, Jr., and P. J. Reynolds, *Monte Carlo Methods in Ab Initio Quantum Chemistry* (World Scientific, Singapore, 1994).

[31] L. Vranješ and S. Kilić, Phys Rev A **65**, 042506 (2002).